Strong Field Electron Emission from Fixed in Space H_{2}^{+} Ions

M. Odenweller, N. Takemoto, A. Vredenborg, K. Cole, K. Pahl, J. Titze, L. Ph. H. Schmidt, T. Jahnke, R. Dörner, and A. Becker

Phys. Rev. Lett. **107**, 143004 — Published 28 September 2011

DOI: 10.1103/PhysRevLett.107.143004

Strong field electron emission from fixed in space H_2^+ ions

M. Odenweller,[1] N. Takemoto,[2,*] A. Vredenborg,[1] K. Cole,[1] K. Pahl,[1]
J. Titze,[1] L. Ph. H. Schmidt,[1] T. Jahnke,[1] R. Dörner,[1] and A. Becker[2]

[1] *Institut für Kernphysik, J. W. Goethe-Universität, Max-von-Laue-Str.1, 60438 Frankfurt am Main, Germany*

[2] *JILA and Department of Physics, University of Colorado, 440 UCB, Boulder, CO 80309-0440, USA*

We have studied electron emission from the H_2^+ ion by a circularly polarized laser pulse (800 nm, 6×10^{14} W/cm^2). The electron momentum distribution in the body fixed frame of the molecule is experimentally obtained by a coincident detection of electrons and protons. The data are compared to a solution of the time-dependent Schrödinger equation in two dimensions. We find radial and angular distributions which are at odds with the quasi-static enhanced ionization model. The unexpected momentum distribution is traced back to a complex laser driven electron dynamics inside the molecule influencing the instant of ionization and the initial momentum of the electron.

PACS numbers: 33.80.Rv,42.50.Hz,32.80.Rm

The interaction of ultrashort strong laser pulses with matter gives rise to a wealth of phenomena, including the generation of higher order harmonics [1, 2] and attosecond pulses [3–5], (coherent control of) molecular dissociation [6, 7], ultrafast molecular imaging [8–10], electron diffraction [11, 12] and angular streaking [13]. For all these phenomena ionization by the laser field is the doorway step. Widely-used ionization pictures are based on the quasi-static approximation of the laser field. In tunnel ionization the combined potential of the Coulomb attraction of the atomic or molecular core and the laser electric field form a barrier through which the electron can escape. Some molecules, such as H_2^+, show more complex ionization mechanisms. Due to a strong coupling between two quasi-degenerate states (so called, charge-resonant states) in H_2^+ at intermediate internuclear distances the energy level is lifted at one of the protons and decreased at the other by the laser electric field. At high field strengths the upper state lies above the internal Coulomb barrier and the electron is ionized efficiently (called enhanced ionization, [14, 15]). All these quasi-static ionization pictures have in common that the ionization probability is expected to be largest whenever the external field is strongest. The escaping electron is assumed to be accelerated by the field. The final momentum is obtained as $\mathbf{p}_f = q_e\mathbf{A}(t_i) + \mathbf{p}_i$ [16], where $q_e = -e$ is the electron charge, $\mathbf{A}(t_i)$ is the vector potential at the instant of ionization t_i, and $\mathbf{p}_i$ is the initial electron momentum, which is often assumed to be negligible.

In our study, ionization is reexamined for the hydrogen molecular ion, which is an ideal system for theoretical analysis because of the absence of the electron-electron correlation effect. Experimentally, however, observation of the full electron-nuclear dynamics from H_2^+ poses a major challenge. In most previous studies the ions are produced from the neutrals by the laser pulse itself. Then, however, the electron emitted in this preparatory step cannot be distinguished from the electron of interest, emitted from the ion. Therefore, we have performed the experiment using a fast ion beam from an accelerator, as it is common for studies of dissociation [17–19]. Electron momentum imaging together with retrieval of the molecular axis and the internuclear distance at the instant of electron ejection requires a coincidence measurement of the momenta of all particles. Such a measurement is highly demanding in a laser-ion crossed beam experiment. Our results show that resolving the electronic dynamics of strong-field ionization of a molecule provides complementary information to earlier experiments which capture the slower nuclear dynamics only [20]. We find that, surprisingly, the standard ionization picture fails. The electron is emitted from the molecular ion at time instants and with momenta which do not concur with the common expectations. Finally, we show how observation of the electron momenta in the continuum provide insights into the laser-driven electron dynamics inside the molecule on an attosecond time scale.

The present experiment was performed at the Van-de-Graaff accelerator of the Stern-Gerlach-Zentrum of the J.W. Goethe-Universität Frankfurt. H_2^+ is produced in a high frequency ion source and accelerated to 400 keV. As the ion beam is not cooled the distribution of vibrational states is due to a Franck-Condon transition from the electronic and vibronic ground state of the neutral H_2 molecules [21]. The ion beam is overlapped with a circularly polarized 8 kHz, 35 fs (13 cycles), 780 nm laser pulse of peak intensity 6×10^{14} W/cm^2. The laser is set up at an angle of 20 degrees with respect to the ion beam. The focus has a diameter of 31 μm and a length of 1.9 mm. A homogeneous electric field of 36 V/cm perpendicular to the ion beam direction guides the electrons created in the laser focus towards a 120 mm active diameter position sensitive microchannel-plate detector with delay line position readout [22]. The electron detector is placed parallel to the ion beam at 5 cm distance and shifted downstreams (in direction of the ion beam) by 11 cm with respect to the laser focus. This downstream shift avoids that electrons emitted from the ion-

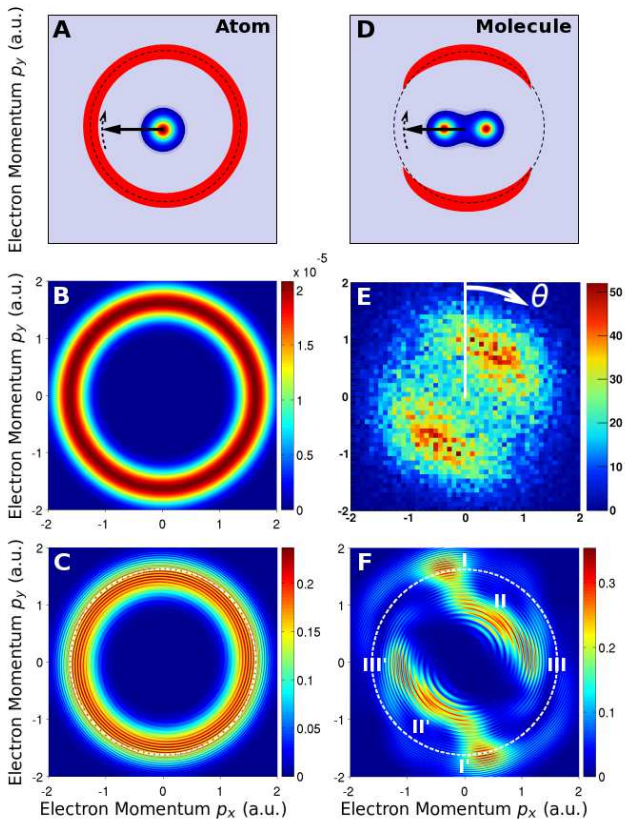

FIG. 1. Photoelectron momentum distribution from an atom (panels A-C) and a molecule (panels D-F) in a circularly polarized laser pulse at 6×10^{14}W/cm^2. (A) Expected ring distribution with radius given by the maximum value of the vector potential A_0 for an atom (dashed line), (B) predictions of the ADK theory [23] and (C) result of a TDSE simulation for a two dimensional model of He^+ atom. (D) Expected distribution for emission from H_2^+, (E) experimental result for H_2^+ integrated over the internuclear distance R and p_z and (F) result of a TDSE simulation for a two dimensional model of H_2^+ at $R = 7$ a.u.. Contributions I, II, and III (and I', II', III') correspond to three different ionization events (see text).

ization of residual gas by the laser hit the detector, while those emitted in the moving frame of the fast H_2^+ beam are collected with 4π solid angle onto the detector. The protons are detected 3 m downstream of the laser focus by a second position sensitive microchannel-plate detector with delay line position readout. For protons and electrons the times-of-flight and positions of impact were recorded event by event in coincidence. The final electron momenta in the body fixed frame of the molecule were calculated from these data. The internuclear distance R at the instant of ionization is calculated from the kinetic energy release (KER) of the protons. In the intense laser pulse, H_2^+ first starts to dissociate and is ionized most likely as the internuclear separation reaches $R = 5$-12 a.u. [14, 15]. At shorter internuclear distances, $R < 5$ a.u., nearly no ionization events were observed. The contribution of this dissociation process on the measured KER and the calculated R is taken into account.

For a pulse length of 13 cycles, the magnitudes of the electric field $\mathbf{E}(t)$ and the vector potential $\mathbf{A}(t)$ are almost constant over several laser periods near the peak and only their directions rotate. If an atom with a spherical symmetric electron probability density is placed in this field, an electron is released at a constant rate as the field rotates. The simple man model [16] predicts a donut shaped final electron momentum distribution of radius $|\mathbf{p}_f| = |q_e A_0|$, where A_0 is the peak amplitude of the vector potential (cf. illustration in Fig. 1(A)). This expectation agrees with the results of the quasi-static ionization theory [23] (Fig. 1(B)) as well as the result of a numerical solution for the time-dependent Schrödinger equation (TDSE) (Fig. 1(C)), and recent observations [24]. In the case of H_2^+ the ionization rate is expected to be largest when $\mathbf{E}(t)$ is aligned along the symmetry axis of the molecule. Therefore, the photoelectron momentum distribution is expected to peak perpendicular to the molecular axis on the ring, $|\mathbf{p}_f| = |q_e A_0|$ (Fig. 1(D)) [25]. However, we experimentally observe the momentum distribution tilted in the same direction (clockwise) as the rotation of the laser field (Fig. 1 (E)) and peaked at lower radial momenta than expected. The electron momentum distribution is shown in the molecular frame where the molecular axis lies along the horizontal axis and the data are integrated over R.

The features of the experimental data are reproduced as the main contribution in the result of our numerical simulation (peaks II and II' in Fig. 1(F)). We solved the TDSE for a two dimensional model of H_2^+ in which the motion of the electron in the polarization plane of the laser field is taken into account while R is fixed. A soft-core parameter was used to closely reproduce the ground and first excited state energies of actual H_2^+. The momentum-space wave function was calculated at the end of the pulse by the Fourier transform of the ionized part of the wavefunction. The latter was obtained by smoothly masking out the bound part of the wave function near the protons. The momentum distribution in Fig. 1(F) was obtained from the simulation at $R = 7$ a.u. after interaction with a circularly polarized laser pulse having a peak intensity of 6×10^{14} W/cm^2, a wavelength of 800 nm, a FWHM pulse duration of 4 cycles and a $\sin^2$-shaped envelope.

Fig. 2(A) shows that the tilt angle θ, measured from the expected direction perpendicular to the molecular axis in the sense of rotation of the laser field (cf. Fig. 1(E)), increases as R increases both in experiment and theory. At the same time, Fig. 2(B) shows that the magnitude of the electron momentum decreases as R increases. Clearly, both observations are at odds with the predictions by the quasi-static model (dashed lines).

To compare experiment and theory in more detail, in

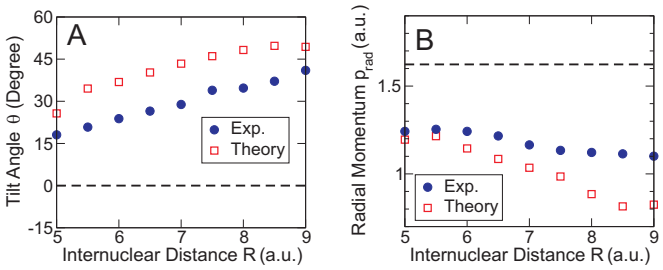

FIG. 2. Dependence of the tilt angle (A) and the mean radial momentum (B) on R. Dashed lines: predictions of simple quasi-static model, blue filled circles: experimental data, red open squares: results of TDSE calculations.

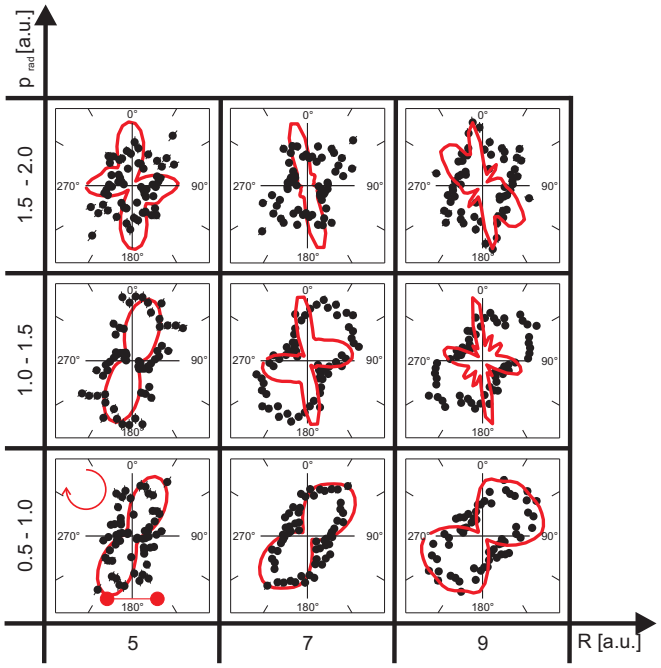

FIG. 3. Angular distributions of the experimental data (black dots) and theoretical results (red solid line) for a clockwise circularly polarized laser pulse of intensity 6×10^{14} W/cm^2. The experimental data are integrated over p_z. The internuclear axis is set along the x-axis. The columns correspond to $R = 5$ a.u., $R = 7$ a.u. and $R = 9$ a.u. from left to right, and the rows to different regions of electron radial momenta.

Fig. 3 we present polar plots of the photoelectron momentum angular distribution at three internuclear separations and in three regions of electron radial momentum. The dominant, tilted, contributions corresponding to peaks II and II' in Fig. 1(F) are captured in the lowest radial momentum section at each internuclear distance, and the experimental and simulation results agree on the tilt angle as well as the width of the angular distribution. With increasing radial momentum (upper two rows in Fig. 3) this main contribution fades away in the theoretical data and other but weaker contributions appear in the directions of $-30° < \theta < 0°$ and $75° < \theta < 150°$, which correspond to peaks I and III in Fig. 1(F), respectively. In contrast, in the experimental results the main contribution spreads out to higher momenta making the other contributions much less pronounced. The discrepancies could be due to the fact that the soft-core Coulomb potential and the energy level structure in the 2D model differ from the real H_2^+. The electron dynamics in the molecular ion, which affects the timing of the ionization (see below), is likely to be sensitive to details of the level structure. Previous calculations [28] for the case of linear polarization indicate that the fixed nuclear assumption does not affect the theoretical results significantly. The different pulse lengths used in experiment and theory could be another origin for the discrepancies.

Next, we elucidate the mechanisms leading to the peaks I-III in Fig. 1(F) by analyzing snapshots of the electron probability density obtained from the numerical results in Fig. 4. In each snapshot, the saddle points of the instantaneous superposition of the Coulomb and laser field potentials are marked by $+$ and $\oplus$. The thick arrow indicates the initial momentum $\mathbf{p}_i = m_e \mathbf{v}_i$ of the electron wavepacket ψ. m_e is the electron mass and $\mathbf{v}_i = \mathrm{Im}\left[\frac{1}{\psi}\nabla\psi\right]$ the local flow velocity at the origin of the arrow. The thin arrow represents the momentum $q_e\mathbf{A}(t_i)$ gained in the laser field according to classical mechanics.

The snapshot Fig. 4(A) captures the time instant when $\mathbf{E}(t)$ is parallel to the molecular axis. The electron wavepacket escapes through the outer saddle point ($\oplus$) with momentum $\mathbf{p}_i$ pointing at an angle of about 70° with respect to $q_e\mathbf{A}(t_i)$. Therefore, this wavepacket ends with a final momentum, $\mathbf{p}_f = q_e\mathbf{A}(t_i) + \mathbf{p}_i$, having a magnitude larger than the expected value of $q_e A_0$ and an angle slightly smaller than the expected 0°. This explains how peak I in Fig. 1(F) is formed.

The snapshot in Fig. 4(B) taken 356 attoseconds (0.133 cycles) later captures an event which is not present in the standard quasi-static enhanced ionization picture. It gives rise to the major contribution in the momentum distribution (peak II), which shows several unexpected features: First, the wavepacket does not leave the molecule over the saddle point, but on the slope of the potential. Second, it has an initial velocity with a component opposite to the acceleration $q_e\mathbf{A}(t_i)$. This explains the small final momenta observed for peak II. Third, the laser field is not aligned along the molecular axis, and the vector potential points to an angle larger than 0°. Consequently, peak II is found under a tilted angle.

The dominant ionization event II is induced due to a strong coupling of the quasi-degenerate ground and first excited states at intermediate internuclear distances. This coupling does not only lead to the phenomenon of enhanced ionization but also generates an attosecond dynamics of the electron population between the two protons in the hydrogen molecular ion [26–28]. The bound

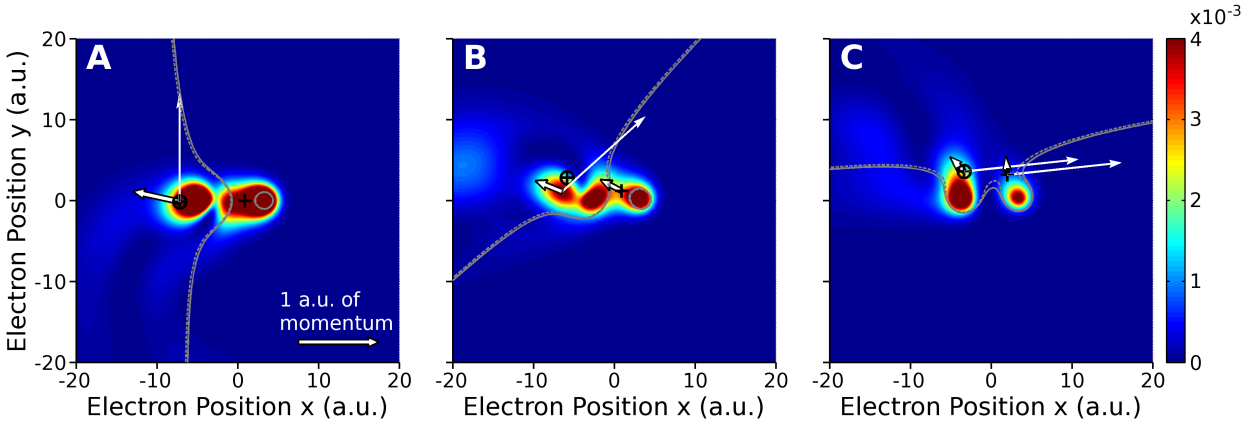

FIG. 4. Snapshots of the calculated electron density in H_2^+ under a circularly polarized laser pulse at $t = t_1 = -1.3 \times 10^{-4}$ laser cycles (a), $t = t_2 = 0.13$ laser cycles (b) and $t = t_3 = 0.23$ laser cycles (c). Time zero is set at a maximum of the x-component of the electric field. The gray solid and dashed lines are the contour lines of the potential at the field free energies of the ground and first excited states, respectively. The + signs mark the saddle points of the instantaneous potential. The bold white arrow with black edge indicates the initial momentum $\mathbf{p}_i$ at the origin of the arrow, and the thin white arrow indicates $q_e\mathbf{A}(t)$. The two protons are placed at $(x, y) = (\pm 3.5\text{a.u.}, 0)$).

wavepacket is transferred to one of the protons only after $\mathbf{E}(t)$ was aligned along the molecular axis. This attosecond time lag and the initial substantial momentum in the electron emission are directly mapped onto the increasing tilt angle and the decreasing magnitude of the final momentum distribution, respectively (Fig. 2).

Finally, in Fig. 4(B) there is a part of the density flowing from the right proton through the saddle between the two protons. This contribution forms the density at the outer part of the snapshot in Fig. 4(C), which is then wiped off the molecule as the electric field vector further rotates, leading to the weak contribution III (Fig. 1(F)).

In conclusion, our study shows that the standard enhanced ionization picture needs to be revised for the simplest molecular system. The observed unexpected time instants and initial velocities for the electron emission are due to a complex electronic motion inside H_2^+. In a broader context our works shows the exciting prospect that the dynamics of an electron inside a molecule on the attosecond time scale can be mapped onto the momenta in the continuum where they become observable.

The experimental work was supported by the Deutsche Forschungsgemeinschaft. We thank K. Stiebing, P. Ziel, M. Dworak, and W. Dilfer for providing an excellent ion beam. The theoretical work was supported by the U.S. National Science Foundation and the U.S. Department of Energy.

* Present Address: Department of Chemical Physics, Weizmann Institute of Science, 76100 Rehovot, Israel

[1] A. McPherson et al., J. Opt. Sco. Am. B **4**, 595 (1987)
[2] Z.H. Chang et al., Phys. Rev. Lett. **79**, 2967 (1997)
[3] P. Christov et al., Phys. Rev. Lett. **78**, 1251 (1997)
[4] M. Hentschel et al., Nature **414**, 509 (2001)
[5] P.M. Paul et al., Science **292**, 1689 (2001)
[6] L. Zhu et al., Science **270**, 77 (1995)
[7] A. Assion et al., Science **282**, 919 (1998)
[8] J. Itatani et al., Nature **432**, 867 (2004).
[9] W. Li et al., Science **322**, 1207 (2008)
[10] W. Li et al., Proc. Natl Acad. Sci. USA **107**, 20219 (2010).
[11] M. Meckel et al., Science **320**, 1478 (2008)
[12] D. Ray et al., Phys. Rev. Lett. **100**, 143002 (2008)
[13] P. Eckle et al., Science **322**, 1525 (2008).
[14] T. Zuo and A. D. Bandrauk, Phys. Rev. A **52**, R2511 (1995).
[15] T. Seideman, M. Yu. Ivanov, P. B. Corkum, Phys. Rev. Lett. **75** 2819 (1995).
[16] According to classical mechanics and neglecting the Coulomb attraction of the nuclei, see P. B. Corkum, N. H. Burnett, and F. Brunel, Phys. Rev. Lett. **62**, 1259 (1989).
[17] K. Sändig, H. Figger, T. W. Hänsch, Phys. Rev. Lett. **85**, 4876 (2000).
[18] D. Pavičić, A. Kiess, T. W. Hänsch, and H. Figger, Phys. Rev. Lett., **94**, 163002 (2005)
[19] I. Ben-Itzhak et al., Phys. Rev. Lett. **95**, 073002 (2005).
[20] A. Staudte et al., Phys. Rev. Lett.**98**, 073003 (2007).
[21] G. Dunn, J. Chem. Phys. **44**, 2592 (1966)
[22] O. Jagutzki, et al., Nucl. Instr. and Meth. in Phys. Res. A **477**, 244 (2002)
[23] N.B. Delone and V.P. Krainov, J. Opt. Soc. Am. B **8**, 1207 (1991).
[24] L. Arissian et al., Phys. Rev. Lett. **105**, 133002 (2010).
[25] A. Staudte et al., Phys. Rev. Lett. **102**, 033004 (2009).
[26] I. Kawata, H. Kono, and Y. Fujimura, J. Chem. Phys. **110**, 11152 (1999).
[27] F. He, A. Becker, and U. Thumm, Phys. Rev. Lett. **101**, 213002 (2008).
[28] N. Takemoto and A. Becker, Phys. Rev. Lett. **105**, 203004 (2010); Phys. Rev. A**84**, 023401 (2011).